Phase Behavior of ABC Triblock Terpolymers in Thin Films: Mesoscale Simulations

S. Ludwigs,* G. Krausch, and R. Magerle*,†

Physikalische Chemie II, Universität Bayreuth, D-95440 Bayreuth, Germany

A. V. Zvelindovsky‡ and G. J. A. Sevink

Leiden Institute of Chemistry, Leiden University, P.O. Box 9502, 2300 RA Leiden, The Netherlands

Received May 14, 2004; Revised Manuscript Received November 21, 2004

ABSTRACT: Microphase separation and morphology of thin films of ABC triblock terpolymers are studied with a self-consistent-field theory. Thin films of poly(styrene)-*block*-poly(2-vinylpyridine)-*block*-poly(*tert*-butyl methacrylate) (SVT) triblock terpolymers are modeled as $A_3B_4C_{12}$ Gaussian chains confined in a slit. The bulk morphologies are found to be much more robust with respect to the interaction parameters when compared to the morphologies in the confined situation. By adjusting the interaction parameters between the polymer components and the surfaces, we can model the experimentally observed sequence of surface structures as a function of the film thickness. At well-defined film thicknesses a highly ordered perforated lamella structure is observed. We systematically explore the influence of film thickness, surface field, and the interaction parameters between the different polymer components on the phase behavior.

Introduction

In recent years it has been shown that ordered block copolymer structures with characteristic sizes in the range of 5−50 nm might be a promising material for lithographic masks, membranes, and quantum electronic arrays.[1−3] In particular thin film structures are of great interest, as long-range ordering of microdomain structures is facilitated.[4−6] In thin films two factors significantly control the structure formation: the preferential attraction of one type of block to the surface (the surface field), which causes this component to accumulate at the interface, and the commensurability of the natural domain spacing with the film thickness.[7−9]

Most theoretical studies on block copolymers in thin films have focused on two-component systems, either AB diblock or symmetric ABA triblock copolymers, which form lamellae in the bulk (for a review, see refs 7−9). Compositionally asymmetric, mostly cylinder-forming block copolymers have been studied only recently. Their phase behavior in thin films has been studied with the Ginzburg−Landau equation,[10,11] cell dynamical simulations,[12] Cahn−Hilliard-type coarse-grained models,[13,14] and Monte Carlo simulations.[15−17] Also, various self-consistent-field (SCF) studies have been performed for the formation of microphases in thin films of cylinder-forming AB diblock and ABA triblock copolymer melts and solutions.[18−22] Recently, Knoll et al. and Horvat et al. have compared experimental results on thin films of poly(styrene)-*block*-poly(butadiene)-*block*-poly(styrene) (SBS) triblock copolymers with SCF simulations for similar interfaces, where the surface fields are equal at both interfaces.[23−25] They could show a matching sequence of structures with increasing film thickness. Lyakhova et al. have additionally investigated the role of dissimilar interfaces on the phase behavior of these block copolymers.[26] In experiments, usually supported films are studied that are asymmetric with respect to interactions at the air−film and film−substrate interfaces.

In contrast to two-component systems, the phase behavior of ABC triblock terpolymers is much more complex, and a much larger number of simulation parameters is needed to describe thin films: the film thickness (H), the volume fractions of the components (ϕ_A, ϕ_B, $\phi_C = 1 - (\phi_A + \phi_B)$), three mutual interaction parameters between the components (ϵ_{AB}, ϵ_{AC}, ϵ_{BC}), and six interaction parameters between the different interfaces and the three components (ϵ_{AM_0}, ϵ_{BM_0}, ϵ_{CM_0}, ϵ_{AM_1}, ϵ_{BM_1}, and ϵ_{CM_1} with M_0 and M_1 representing the top surface and the substrate, respectively).

In the field of ABC triblock terpolymer thin films, Pickett and Balazs have used self-consistent-field calculations to probe the preferential orientation of lamellae formed by an ABC triblock terpolymer confined between two walls attracting the middle block.[27] They found that an orientation of the lamellae perpendicular to the plane of the film orientation is highly favored, indicating that triblock terpolymers possess distinct advantages over diblocks in technological applications. Monte Carlo simulations by Feng and Ruckenstein for ABC melts in thin films show that the microdomain morphology can be very complicated and is affected both by the composition and by the interactions.[28] Finally, Chen and Fredrickson have applied self-consistent-field theory and strong segregation limit studies (SSL) to investigate confined films of linear ABC triblock terpolymer melts[29] for the particular case where A and C blocks are equal in size, the interaction parameters are identical, and both walls have identical chemical properties. Their findings confirm that surface fields and film thicknesses can be employed to manipulate the microdomain structure, shape, and orientation.

In the present contribution we model a specific system of compositionally asymmetric triblock terpolymers

† Present address: Institut für Physik, Technische Universität Chemnitz, D-09107 Chemnitz, Germany.

‡ Present address: Centre for Materials Science, Department of Physics, Astronomy & Mathematics, University of Central Lancashire, Preston, PR1 2HE, United Kingdom.

* Corresponding authors. E-mail: sabine.ludwigs@uni-bayreuth.de or robert.magerle@physik.tu-chemnitz.de.

10.1021/ma049047l CCC: $30.25
Published on Web 02/03/2005

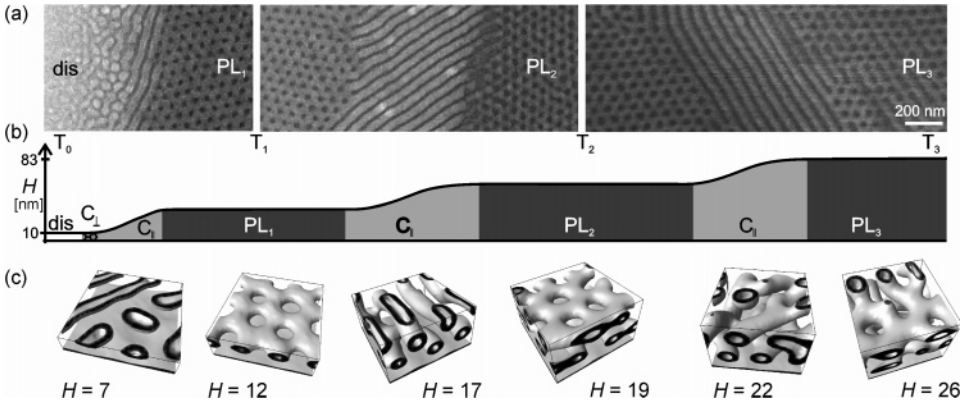

Figure 1. Comparison of experiments with simulation results. (a) Scanning electron micrographs of a thin film of a poly(styrene)-*b*-poly(2-vinylpyridine)-*b*-poly(*tert*-butyl methacrylate) triblock terpolymer ($S_{17}V_{22}T_{61}^{132}$) on a silicon substrate after annealing in chloroform vapor. (b) Schematic height profile of the electron micrographs shown in (a). (c) Simulations of an $A_3B_4C_{12}$ block terpolymer film. The isodensity surfaces of the B density ρ_B are shown for different film thicknesses H. The mutual interaction parameters between the block components are $\epsilon = (\epsilon_{AB}, \epsilon_{AC}, \epsilon_{BC}) = (7.0, 8.0, 6.0)$. The block−surface interactions are $\epsilon_{M_0} = (\epsilon_{AM_0} + \epsilon_{BM_0})/2 - \epsilon_{CM_0} = 5.0$ (M_0 = top surface) and $\epsilon_{M_1} = (\epsilon_{AM_1} + \epsilon_{BM_1})/2 - \epsilon_{CM_1} = -5.0$ (M_1 = silicon substrate).

Table 1. Experimental Results: Bulk Morphologies[30]

polymer[a]	ϕ_{PS}:ϕ_{P2VP}:ϕ_{PtBMA}[b]	bulk morphology[c]
$S_{19}V_{25}T_{56}^{120}$	1:1.2:3.05	G/PL/C
$S_{18}V_{24}T_{58}^{124}$	1:1.2:3.33	G/PL/C
$S_{17}V_{23}T_{60}^{129}$	1:1.2:3.53	G/PL/C
$S_{17}V_{22}T_{61}^{132}$	1:1.2:3.65	G/PL/C
$S_{16}V_{21}T_{63}^{140}$	1:1.2:4	C

[a] $S_{\%PS}V_{\%P2VP}T_{\%PtBMA}^{M_w}$ with the subscripts representing the weight fractions of the respective blocks (parts in hundred), while M_w is the total weight-averaged molecular weight in kg/mol. [b] ϕ_{PS}:ϕ_{P2VP}:ϕ_{PtBMA}, volume fractions. [c] Key: G, core−shell gyroids; PL, perforated lamellae; C, core−shell cylinders.

consisting of poly(styrene) (PS), poly(2-vinylpyridine) (P2VP), and poly(*tert*-butyl methacrylate) (PtBMA) in a thin film. We relate to a corresponding experimental investigation of the behavior of this material in bulk[30] and in thin films.[31,32]

Using combinatorial gradient techniques, Ludwigs et al. have systematically explored the dependence of thin film structures of PS-*b*-P2VP-*b*-PtBMA with volume fractions ϕ_{PS}:ϕ_{P2VP}:$\phi_{PtBMA} = 1:1.2:x$ (with x ranging from 3.05 to 4) on the film thickness and preparation conditions.[32] Depending on the volume fraction of PtBMA either core−shell cylinders (ϕ_{PS}:ϕ_{P2VP}:$\phi_{PtBMA} = 1:1.2:4$) or a coexistence of core−shell gyroids, core−shell cylinders and a perforated lamella structure (ϕ_{PS}:ϕ_{P2VP}:$\phi_{PtBMA} = 1:1.2:3.05-3.63$) are found in the bulk. Table 1 summarizes the molecular parameters of the experimentally investigated polymers.

For thin film investigations, polymer films with gradients in film thickness were annealed in a controlled chloroform vapor atmosphere, quenched with pure air, and investigated with scanning electron microscopy and scanning force microscopy.[32] The structure formation process takes place in concentrated solutions. While experiencing different morphologies in bulk as a function of the composition, the microdomain structures in thin films are very similar for the whole range of ϕ_{PtBMA} from ϕ_{PS}:ϕ_{P2VP}:$\phi_{PtBMA} = 1:1.2:3.05-4.0$. Figure 1a shows scanning electron micrographs of a thin film of $S_{17}V_{22}T_{61}^{132}$ annealed in $CHCl_3$ with a film thickness of ∼10−80 nm. The dark phase can be attributed to the majority component poly(*tert*-butyl methacrylate), which is known to shrink upon exposure to the electron beam. With increasing film thickness the following sequence of structures is found: a featureless pattern, which is identified as disordered phase (dis), bright dots with liquidlike packing, a stripelike pattern corresponding to parallel oriented core−shell cylinders ($C_{||}$). The terraces exhibit a hexagonally packed structure of dark dots, which is identified as a perforated lamella phase (PL). At the slopes between the terraces $C_{||}$ is found. For a detailed discussion we refer to the accompanying experimental paper.[32]

We model the thin films as a melt of $A_3B_4C_{12}$ flexible chains confined between two walls, one representing the top surface and the other representing the substrate. The indices correspond to the number of statistical elements (beads) of the same chemical species, and they correspond to the volume fractions of the three components in the polymer. Because of the coarse-grained description of the molecule, we will not distinguish between small variations in the volume fractions, which, in the experiments, have shown to lead to different phases in the bulk. Here, we pick one particular volume fraction and focus on the influence of the energetic interactions between the different components and the interfaces as tunable parameters. The solvent used during the sample preparation in the experiments is accounted for by choosing appropriate interaction parameters based upon comparison of experimental and simulational confined phase diagrams. It was shown earlier that such a description is well justified and gives an excellent agreement with experiments.[23]

With the input of the experiments of Ludwigs et al.[32] and several previous studies about SVT triblock terpolymers performed by Elbs et al.[33−35] and Fukunaga et al.,[36−38] we have adjusted the interaction parameters such as to match the experimental phase behavior observed in the experiments of Ludwigs et al. We present our simulation results for this set of parameters and compare them with the experimental data described in the accompanying article.[32] We also explored the behavior of the system in the vicinity of this parameter set.

Method

We apply a dynamic version of the SCF simulation technique[18,39,40] to model the SVT triblock terpolymers. The block terpolymer is modeled as $A_3B_4C_{12}$ Gaussians chains with different beads A (= poly(styrene)), B (= poly(2-vinylpyridine)), and C (= poly(*tert*-butyl methacrylate)). The relative number of beads coincides with

the volume fractions of the different components in the triblock terpolymer. The total number of beads is small enough to ensure computational efficiency. The spatial patterns are found as numerical solutions of diffusion-type equations for component densities. This type of approach ensures spontaneous pattern formation, natural appearance of defects in structures, and metastable states which is common to the situation in the experiments.

Polymer films on silicon substrates are mimicked as a polymer melt confined between two parallel hard walls. The simulations are performed on a cubic grid with $L \times L \times W$ grid points, with $L = 32$ or 64 and W varying from 6 to 28. The walls are presented as planes at $z = 1$ and W; hence, the film thickness H equals $W - 2$ grid points. The ratio of the bond length between beads and one grid unit is 1.158.[41] For modeling the bulk, periodic boundary conditions apply in all three spatial directions; in the confined case, special boundary conditions apply at the walls.[18]

The interaction strengths between the three components and between the components and the walls are characterized by ϵ_{XY} parameters (in kJ/mol) that are directly related to the more familiar dimensionless Flory–Huggins parameters (given the temperature $T = 413$ K, bond volume $\nu = 1$, and $\epsilon_{XX} = \epsilon_{YY} = 0$).[40] These mean-field interactions are explicitly nonlocal by the choice of a Gaussian interaction kernel in the two-body mean-field potential.[42] As a rule of thumb, a positive (negative) ϵ_{XY} parameter corresponds to an net repulsion (attraction) of the component X and Y. The same holds for the interaction between the walls and the components. The mutual interactions between the different components have been chosen such as to match the bulk structure in the experiments. In the experiments always core–shell microdomain structures are observed; accordingly, we have chosen a strong repulsion between all three components in our simulations.

For thin film investigations we further had to determine the six interaction parameters between the two different walls and the three components: ϵ_{AM_0}, ϵ_{BM_0}, ϵ_{CM_0}, ϵ_{AM_1}, ϵ_{BM_1}, and ϵ_{CM_1} with M_0 representing the top surface and M_1 representing the substrate. We introduce two auxiliary interaction parameter combinations $\epsilon_{M_0} = (\epsilon_{AM_0} + \epsilon_{BM_0})/2 - \epsilon_{CM_0}$ and $\epsilon_{M_1} = (\epsilon_{AM_1} + \epsilon_{BM_1})/2 - \epsilon_{CM_1}$, where the interaction of the A and B components with the walls is being averaged. ϵ_{M_0} and ϵ_{M_1} characterize the strength of the surface field. A positive ϵ_{M_0} and ϵ_{M_1} parameter indicates how much the A and B component (C component) dislike (like) the surface M_0 and M_1, respectively. From the experiment we know that the second block B (P2VP) is strongly adsorbed on polar substrates, like SiO_x, and that the C component, which is the majority component, is at the free surface as it has the lowest interfacial energy toward air. On the basis of this experimentally observed phase behavior, we adjusted the surface interactions in the simulations such that the sequence of surface patterns fits the experimental observations. Starting from this fit we explore how this set of parameters works for other situations.

Results and Discussion

Bulk Phase Behavior. We first compare the simulation results on the phase behavior in bulk with the corresponding experiments. In the experiments, the microdomain structure depends on the composition of the block terpolymer:[30] PS-*b*-P2VP-*b*-PtBMA polymers with a composition of $\phi_{PS}:\phi_{P2VP}:\phi_{PtBMA} = 1:1.2:4$ exhibit core–shell cylinders. Decreasing the volume fraction of PtBMA to values between 3.05 and 3.65 leads to a coexistence of core–shell gyroids, core–shell cylinders, and perforated lamellae.

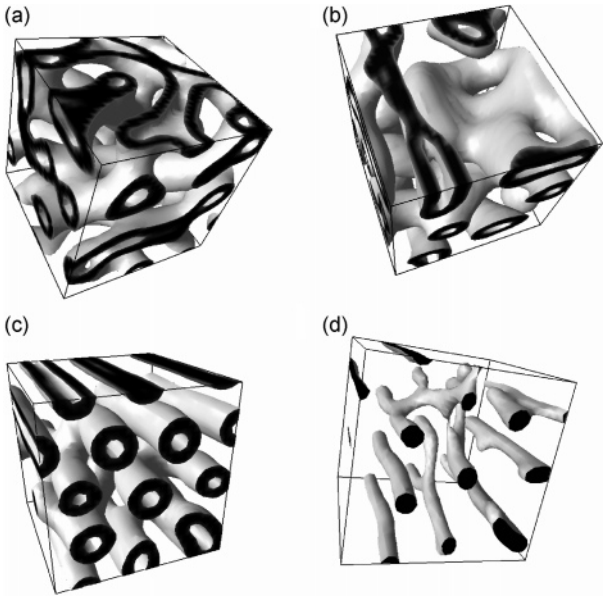

Figure 2. Simulation results for a melt of $A_3B_4C_{12}$ molecules in $32 \times 32 \times 32$ large simulation boxes. The component–component interaction parameters are $\epsilon = (7.0, 8.0, 6.0)$. (a) Isodensity surface of ρ_B after 10 000 steps. (b–d) Effect of shearing. (b) Isodensity surface of ρ_B after shearing for additional 5000 steps (shear rate: 0.001). (c) ρ_B and (d) ρ_A after shearing (b) for additional 15 000 steps (shear rate: 0.002).

The microphase separation process in bulk was simulated on a cubic grid with $L \times L \times L$ grid points. In most simulations, we have considered $L = 32$. The bulk microphase structure was calculated for different values of the mutual interaction parameters $\epsilon = (\epsilon_{AB}, \epsilon_{AC}, \epsilon_{BC})$. Starting from homogeneous density distributions, the calculations were run for 10 000 time steps; from visual inspection we found that during the last 2000 steps no significant changes occurred.

The isodensity surface of the B density ρ_B is shown for $\epsilon = (7.0, 8.0, 6.0)$ in Figure 2a. The structure is difficult to characterize as it still contains many defects. Because of the large amount of three-arm interconnections, the structure resembles a gyroid phase. Investigation of the A and C density shows a core–shell gyroid-like phase with the A component forming the core, surrounded by a shell of the B component embedded in a matrix of the majority component C. Variations of the box size ($L = 24$ and 16) show similar results. This core–shell gyroid structure is found to be robust in a large parameter range (Table 2).

An AB mixed gyroid structure is found when the AB interaction parameter between the two end blocks is decreased to $\epsilon = (6.4, 4.0, 4.5)$. A further decrease of this parameter leads to the coexistence of a gyroid-like structure and cylinders $\epsilon = (6.4, 3.8, 4.5)$ and finally to disordered phases where all three components are mixed $\epsilon = (6.4, \leq 3.0, 4.5)$ (Table 2). As the blocks are much smaller than the C block, the A and B components tend to mix if the energetic penalty is too low.

The stability of the connections, important for the determination of the defected microdomain structure as a gyroid or cylinder structure, can be challenged by the

Table 2. Simulation Results: Bulk Morphologies for Different Interaction Parameters ϵ

ϵ_{AB}	ϵ_{AC}	ϵ_{BC}	morphology[a]	comments
7.0	8.0	6.0	G	core−shell structure
6.0	8.0	7.0	G	core−shell structure
8.0	8.0	6.0	G	core−shell structure
5.0	9.0	6.0	G	core−shell structure
7.0	9.0	7.0	G	core−shell structure
6.4	5.0	4.5	G	core−shell structure
6.4	4.0	4.5	G	A and B mixed
6.4	3.8	4.5	G/C	A and B mixed
6.4	3.0	4.5	dis	A, B, C mixed
6.4	2.0	4.5	dis	A, B, C mixed
6.4	1.0	4.5	dis	A, B, C mixed

[a] Key: G, gyroid-like; C, cylinders; dis, disordered.

application of an external field. Applying a shear field[43] to the core−shell gyroid structure (ϵ = (7.0, 8.0, 6.0)) leads to a partial removal of the interconnections. A perforated lamella-like structure is obtained by shearing with a dimensionless shear rate of 0.001 for additional 5000 steps (Figure 2b) and a cylinder structure by increased shearing with a shear rate of 0.002 for additional 15 000 steps (Figure 2c). As some connections between the cylinders remain after strong shearing for a long period, we conclude that the gyroid structure is most likely to have a slightly lower free energy than the cylinder structure.[43] We conclude that the core−shell gyroid structure, found in a certain composition range in the experiment,[30] is also found in the simulations. The volume fraction considered in the parametrization of the simulation chain is well within this composition range. Moreover, in the simulations, the bulk core−shell gyroid structure seems to be quite stable with respect to rather large variations in the interaction parameter. Upon shearing a perforated lamella and a cylinder phase are found next to the gyroid phase boundaries: an observation which is in line with the experiments, where a coexistence of gyroids, perforated lamellae, and cylinders is found.[30]

Thin Film Phase Behavior. We investigate the phase behavior in thin films as a function of the film thickness. We consider the previous system exhibiting a core−shell gyroid structure in bulk with ϵ = (7.0, 8.0, 6.0). Figure 1 shows the experimental results for $S_{17}V_{22}T_{61}$[132] together with simulations. The scanning electron micrographs in Figure 1a represent the first four terraces (T_0, T_1, T_2, T_3) with increasing film thickness from left to right; the corresponding schematic height profile of the film measured relative to the silicon substrate is shown in Figure 1b.[32] The interaction parameters of the components with the two surfaces are $\epsilon_{M_0} = 5.0$ (M_0 = top surface) and $\epsilon_{M_1} = -5.0$ (M_1 = substrate). With increasing film thickness, both experiments and calculations show the same sequence of surface structures (Figure 1c): The regions with the smallest film thickness (T_0) show a disordered structure (dis), followed by a dotlike structure (which is assigned to $C_\perp$ in the experiments), cylinders oriented parallel to the film plane ($C_{||}$), a perforated lamella structure (PL_1), parallel cylinders ($C_{||}$), a perforated lamella structure (PL_2), parallel cylinders ($C_{||}$), and again a perforated lamella phase (PL_3). The general observation is that terraces exhibit PL, while the slopes between neighboring terraces exhibit $C_{||}$.

The Wetting Layer (W). In the experiments, a featureless layer of approximately 10 nm thickness (T_0) is found in the thinnest regions of a SVT film (see Figure 1a, left part). From measurements of the film thickness and the step height between terraces it was concluded that a wetting layer of similar thickness is formed next to the substrate in thicker films.[32] Elbs et al. and Fukunaga et al. have shown that SVT block terpolymers are pinned onto SiO_x via the polar P2VP (component B in the simulations), while the majority component PtBMA (component C) forms a uniform layer on top.[33,36]

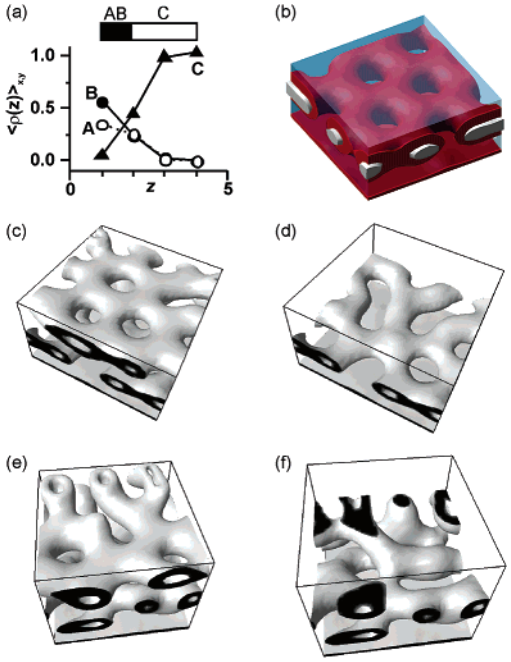

Figure 3. Characteristic surface structures and wetting layer. The interaction parameters are the same as in Figure 2c. (a) Wetting layer. Depth profiles of the laterally averaged densities ρ_A, ρ_B, and ρ_C are shown as a function of the distance z from the surface for $H = 4$. (b−f) Perforated lamella phase. (b) The isodensity surfaces of all three components are shown. The A component forms the core (white) embedded in a shell of the B component (red phase) in a matrix of the C component (blue). (c, d) The isodensity surfaces of ρ_B are shown for H = 19 before and after removing the top layer of PL, respectively. (e, f): Same as (c) and (d) for $H = 16$.

To elucidate the structure in very thin films (four grid cells) in the simulations, we have calculated depth profiles of the laterally averaged densities as a function of the distance z from the surface (Figure 3a). The A and B component are accumulated close to the substrate M_1 at $z = 0$. The A density follows the B density, and a thin AB mixed wetting layer is formed at the substrate ($z = 0$), terminating in a microphase-separated C-rich layer. The mixing of A and B close to the substrate is attributed to the confinement and the rather small fractions of A and B compared to the majority component C ($A_3B_4C_{12}$). The AB mixing is in line with previous observations for AB and ABA block copolymers,[23,25,26] where for very small thickness (H < microdomain spacing) confinement prevents microphase separation and stabilizes a disordered phase.

Regardless of the film thickness, both experiments and simulations show a wetting layer W next to the substrate terminating with a homogeneous layer of the matrix component C. All thin film microdomain structures are formed on top of this AB−C layer. The wetting layer effectively reduces the film thickness and gives rise for an effective interface with strong C character for the reduced film, causing a screening effect.[19,25,26,44] W screens the substrate from the reduced part of the

film, and the surface field at the effective interface is effectively the one that would result from a C-coated surface.

The PL Phase. At well-defined film thickness a perforated lamella structure is found at the top surface in both experiments and simulations. This structure can be described as a P2VP/PS/P2VP sheet perforated by hexagonally arranged PtBMA channels, which connect between two outer PtBMA layers. The PL phase appears at film thickness $H = 12$, 19, and 26 grid points, and the thickness of one single layer of PL amounts to $\Delta H = 7$ grid points. The distance between next-nearest perforations in the PL phase amounts to 10 ± 1 grid points. The characteristic microdomain distances between the PL and the $C_{||}$ phase show an epitaxial relationship similar as in the two-component system.[23,25] As mentioned above, the morphology is formed on top of a wetting layer with a thickness of about five grid points; the wetting layer terminates with the C component. Figure 3b visualizes the isodensity surfaces of all three components for the first terrace of PL. The A, B, and C components are microphase-separated; A and B form a core−shell structure.

In experiments, it was impossible to determine whether the PL structure continues through the depth of the film to the substrate in higher terraces.[32] In the simulations, it is easy to look beneath the top surface. Figure 3c−f shows isodensity surfaces of ρ_B at $H = 19$ (PL_2) and $H = 26$ (PL_3) before and after removing the top PL layer. At $H = 19$ (corresponding to the second terrace T_2) a defective PL structure forms beneath the top PL layer, while at $H = 26$ a gyroid-like network is found beneath the top PL layer.

Our results for $H = 26$ indicate that the surface field extends into the bulk of the film with a decay length of about one microdomain spacing, similar as found in previous investigations.[21,25,26] In thicker films the bulk structure (core−shell gyroids) becomes energetically favored in the center of the film, as the confinement effect becomes less important. The PL phase appears as a surface reconstruction[45] of the gyroid phase.

The $C_{||}$ Structure. In the experiments, the slopes between neighboring terraces exhibit cylinders oriented parallel to the surface ($C_{||}$). Parts a and d of Figure 4 show scanning electron micrographs on areas that include T_1 and the slopes toward T_0 and T_2, respectively. The majority component PtBMA always appears as dark phase, while the other two components show similar contrast (even with staining); for further details see the accompanying article.[32] In the experiments the inner structure of the cylinders cannot be resolved clearly. Core−shell cylinders are either embedded in a PtBMA matrix with a thin layer of PtBMA on top (full cylinders) or all three components are at the free surface which then would be identified as a half-open cylinder. From Figure 4a one may get the impression that there is an inner structure between two dark stripes (PtBMA), but this might also be an artifact of the scanning conditions during imaging with scanning electron microscopy.

Simulations provide a means to interpret the experimentally observed surface structures. Figure 4b,e shows the isodensity surfaces of the B density at $H = 10$ and $H = 14$ in large simulation boxes ($L = 64$). To compare them with the experimental images (a) and (d), we have periodically tiled four two-dimensional slices showing the B density in the top parts of (b) and (e) in parts c and f of Figure 4, respectively. Stripe patterns ($C_{||}$) and

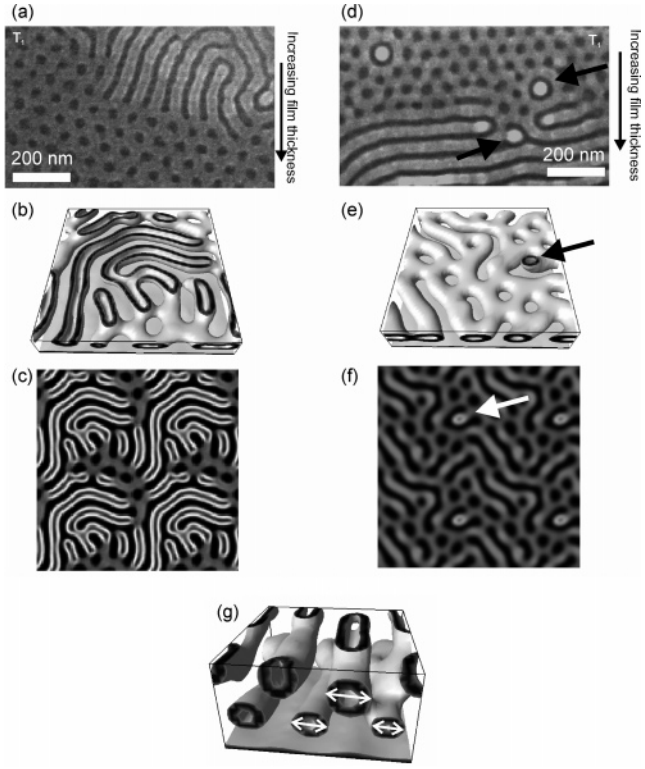

Figure 4. Cylinders in the slopes between terraces. (a, d) Experiments. SEM images of the transition between T_0 and T_1 and between T_1 and T_2. (b, c, e−g) Simulation results. The interaction parameters are the same as in Figure 2c. The isodensity surfaces of the B density are shown for a box size of $L \times L \times H = 64 \times 64 \times 10$ in (b) and a box size of $L \times L \times H = 64 \times 64 \times 14$ in (e). (c, f) Two-dimensional slices of ρ_B in the vicinity of the surface in (b) and (e), respectively. For visualization purposes we have periodically tiled four images of (b) and (e). (g) Isodensity surface of the B density for a box size of $L \times L \times H = 32 \times 32 \times 17$.

perforated lamellae are observed to coexist with the stripes connecting to the PL. The three components are microphase-separated. In thinner films ($H = 10$) half cylinders are favored with all three components at the top surface, and in thicker films ($H = 14$) full cylinders are energetically favored. The thickness of a half cylinder is not the half of that of a full cylinder.

Further details, where simulations and experiments match extremely well, are droplike defects which are marked with arrows in Figure 4d−f.

Figure 4g shows the isodensity surface of ρ_B for a thicker film ($H = 17$). Two layers of core−shell cylinders can be seen. In thicker films we often observe a coexistence of half-open and full cylinders in the top layer. Both simulation results, half and full cylinders, are compatible with the experimental observation where these two situations cannot be distinguished.

In the previous work of Lyakhova et al., half-open structures at the surfaces were identified as a structured wetting layer.[26] In contrast to the findings for ABC systems, these wetting layers always developed as a completely disconnected layer from the bulk of the film, with a fixed thickness.

The cylinders in Figure 4g are hexagonally packed, but there are some interconnections between the two layers. The arrows in Figure 4g mark another important finding: the cylinder radius is quite flexible and adjusts itself to different thicknesses. Lyakhova et al. have recently reported about this phenomenon for a cylinder

forming ABA system with asymmetric surface interaction: they have found that cylinders can even adjust their shapes.[21] This explains why we find cylinders in a large thickness range. In the experiments the same tendency is observed: while cylinders appear over a large thickness range at steps between terraces, the PL phase appears only at well-defined film thicknesses.[32] In accordance to previous publications,[23−26] we can conclude that PL are less deformable than cylinders.

Comparison to the Phase Behavior of Cylinder-Forming ABA Systems. Recently Knoll et al. and Horvat et al. have presented a comparison of the phase diagram for thin films of a cylinder-forming poly(styrene)-*b*-poly(butadiene)-*b*-poly(styrene) triblock copolymer and simulations of a corresponding $A_3B_{12}A_3$ triblock copolymer film, where the interfaces preferentially attract the B component.[23−25] With increasing film thickness, both experiments and calculations show the same sequence of thin film phases: a disordered film (dis) for the smallest film thickness, very short upright cylinders ($C_\perp$), A cylinders oriented parallel to the film plane ($C_{||,1}$), a perforated A lamella (PL), parallel oriented A cylinders with an elongated cross section and necks, perpendicular oriented A-cylinders, and finally two layers of two parallel oriented A cylinders ($C_{||,2}$). An orientation of the microdomains parallel to the film plane is dominant in films with surfaces having a preference for one of the blocks of the copolymer.[19] At incommensurate film thicknesses, however, $C_\perp$ is formed.

Our observations are in qualitative agreement with the main conclusions of the cylinder-forming ABA system. For a system forming a core−shell gyroid structure in bulk, we observe in thin films analogous core−shell PL and $C_{||}$ surface structures with the same sequence of surface structures as a function of the film thickness. While in the ABA system $C_{||}$ appears at commensurate film thickness, we find perforated lamellae at commensurate film thickness. Our core−shell PL is a surface reconstruction of the core−shell gyroid structure, which is induced by the planar symmetry of the surface. In the case of the ABA system, the PL appears due to the strong surface field. At intermediate film thicknesses (in experiments at the slopes between neighboring terraces), we observe $C_{||}$ which can be either half or full cylinders. In thicker films the parallel-oriented cylinders are hexagonally packed, but they show interconnections between layers of cylinders, which is indicative for the gyroid structure in bulk. In very thin films we observe a liquidlike distribution of isolated microdomains in both the experiments and the simulations, which is analogous to the very short upright cylinders ($C_\perp$) observed in the cylinder-forming ABA systems, where the packing was better ordered.

All these findings are illustrative of the fact that the thin film phase behavior of ABC triblock terpolymers is analogous, but more complex than that of ABA block copolymers.

Influence of Surface Field. We further study the influence of the surface field on the surface structures as a function of the film thickness. We again consider the system which forms a core−shell gyroid structure in the bulk ($\epsilon = (7.0, 8.0, 6.0)$). As the phase behavior is very complex, we restrict ourselves to a rather limited region of the phase diagram around the parameter values that we fitted to the experimental data. Starting from these component−surface interactions, we vary the interactions ϵ_{AM_0} and ϵ_{BM_0} of the A and B component with the top surface. As we already mentioned, changing the interactions of the components with the substrate has little influence on the thin film structures due to the wetting layer and its screening effect. Additionally, we consider the case with symmetric walls where no wetting layer is formed at the substrate.

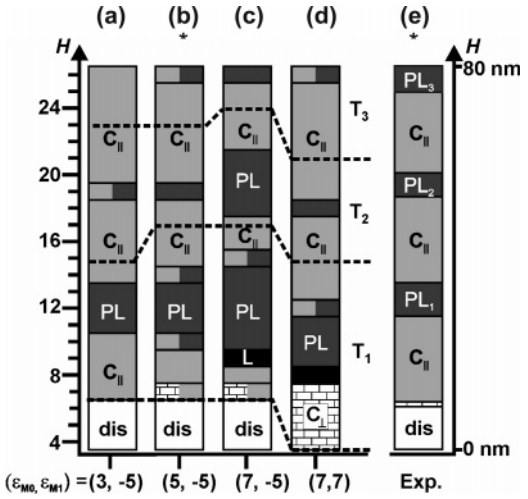

Figure 5. Influence of surface field. Surface structures (close to the free surface) as a function of the film thickness and the interaction parameters with the walls (ϵ_{M_0}, ϵ_{M_1}). Color code: white, dis; light gray, $C_{||}$; dark gray, PL; black, L; tiled, $C_\perp$. The dashed lines indicate the transition from one (two) layer(s) of microdomain structures to two (three) layers. The interaction parameters between the components are set to $\epsilon = (7.0, 8.0, 6.0)$. The interaction parameters with the walls are $(\epsilon_{M_0}, \epsilon_{M_1}) = (3.0, -5.0)$ in (a), $(5.0, -5.0)$ in (b), $(7.0, -5.0)$ in (c), and $(7.0, 7.0)$ in (d). (e) Experimental phase diagram of $S_{17}V_{22}T_{61}$,[132] corresponding to Figure 1b.

Parts b and e of Figure 5 show the sequence of surface structures observed in the simulations and in the experiments as a function of the film thickness, respectively, for the system investigated in the previous subsection of this paper ($\epsilon_{M_0} = 5.0$, $\epsilon_{M_1} = -5.0$). The experimental H axis was scaled such to match the H scale of the simulations. Some of the surface structures have been presented in Figures 2c, 3, and 4. The interaction parameters in the simulations have been chosen such that the sequences of phases of the model and the experiments match.

A decrease of the repulsion of components A and B from the top surface to $\epsilon_{M_0} = 3.0$ leads to the following sequence of surface structures: dis, $C_{||}$, PL_1, $C_{||}$, coexistence of $C_{||}$ and PL_2, and $C_{||}$ (Figure 5a). Compared to the phase diagram of Figure 5b, two effects occur as a result of the weaker surface field: At $H = 7$, $C_\perp$ disappears, and the stability region of $C_{||}$ grows, leading to the disappearance of the coexistent $C_{||}$/PL phase in thinner films at $H = 10$ and $H = 14$. Furthermore, the PL phase in thicker films, at $H = 19$, coexists with $C_{||}$.

Stronger repulsion of A and B from the top surface ($\epsilon_{M_0} = 7.0$) leads to the sequence of surface structures shown in Figure 5c: dis, coexistence of $C_\perp$ and $C_{||}$, $C_{||}$, L, PL_1, coexistence of PL_1 and $C_{||}$, $C_{||}$, PL_2, $C_{||}$, and PL_3. We observe a significant increase of the stability region of PL. Additionally, in thinner films a lamella phase is formed between the $C_{||}$ and PL_1 phases, at $H = 9$. Figure 6a shows the corresponding depth profiles of the different components for $H = 9$. On top of the wetting layer at the substrate, a lamella is formed within which the A and B components are mixed. Such a lamella is also found in the experiments: A thin film of $S_{17}V_{22}T_{61}$[132]

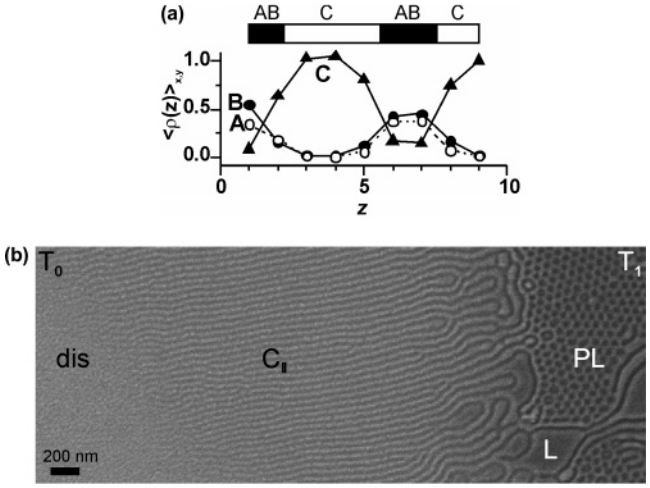

Figure 6. Details and evidence for the lamella phase in the phase diagram of Figure 5c. (a) Depth profiles of the laterally averaged densities ρ_A, ρ_B, and ρ_C for $H = 9$. (b) Experiment: scanning electron micrograph of $S_{17}V_{22}T_{61}^{132}$ prepared on a mica substrate.

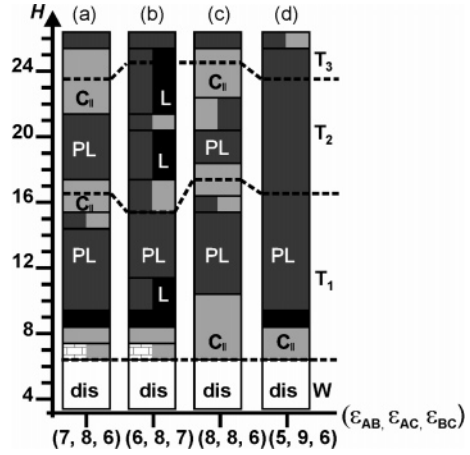

Figure 7. Influence of component−component interaction parameters ϵ on thin film structures as a function of the film thickness. Color code: white, dis; light gray, $C_{||}$; dark gray, PL; black, L; tiled, $C_{\perp}$. The interaction parameters with the walls are set to $\epsilon_{M_0} = 7.0$ and $\epsilon_{M_1} = -5.0$. The interaction parameters between the components are $\epsilon = (7.0, 8.0, 6.0;)$ in (a), (6.0, 8.0, 7.0) in (b), (8.0, 8.0, 6.0) in (c), and (5.0, 9.0, 6.0) in (d).

on mica exhibits $C_{||}$ and L between the disordered region and PL_1.

Regarding the three phase diagrams (Figure 5a−c) we can identify general tendencies. We observe a complex interplay between the surface fields, prominent in the case of very thin films due to the additivity, and confinement effects such as commensurability, which lead to PL structures at film thicknesses that are a multiple amount of natural domain distances. In films with $H > 9$ grid points, only $C_{||}$ and PL are stable surface structures. With increasing surface field at the top surface, the stability region of the PL phase increases and $C_{||}$ are suppressed. In very thin films ($H < 9$) the effect of the surface field has a stronger influence on the surface structures. Increasing the surface field leads to the formation of $C_{\perp}$ between dis and $C_{||}$ (Figure 5c) and to the formation of an AB-mixed lamella L between $C_{||}$ and PL. In this lamella, mixing of the A and B components is due to a very high repulsion of these blocks from the top surface. The existence of L next to PL has already been observed in two-component systems.[21−23,25,26] The fact that the L and the $C_{\perp}$ phase are only observed for thinner films is attributed to the additivity of the surface fields of both surfaces, leading to a combined surface field that exceeds some threshold value necessary for the formation of these structures. This effect is most prominent in thin films, as the surface field extends into the film with a decay length of about one domain distance.[23]

Symmetric Boundary Conditions. To investigate the influence of the wetting layer at the substrate, we also consider a phase diagram for equal component−surface interactions at both walls. Both walls attract the C component, and the surface fields are quite high ($\epsilon_{M_0} = \epsilon_{M_1} = 7.0$). With increasing film thickness we observe the following surface structures: $C_{\perp}$, $L_{||}$, PL_1, coexistence of PL_1 and $C_{||}$, $C_{||}$, PL_2, $C_{||}$, coexistence of PL_3 and $C_{||}$. We note that the phase diagram is rather similar to Figure 5c, except for very thin films, and that the phase boundaries are shifted to lower values of H. In very thin films no $C_{||}$ appear, and the $C_{\perp}$ phase is found in a rather large region of thicknesses, from $H = 4$ to 7. The high surface fields additionally lead to the formation of an AB mixed lamella phase, similar to that of Figure 5c. PL and $C_{||}$ are again observed in the upper part of the phase diagram, with the difference that these structures have much less defects than the structures observed for films with a wetting layer at the substrate.

Comparing parts c and d of Figure 5, we see a clear example of the screening effect: the phase behavior in the presence of a wetting layer and for the system with both surfaces attracting the C component (the symmetric case) is rather similar. In case when the wetting layer is present, it was shown to terminate in a C-rich layer (Figure 3a). When we disregard this wetting layer, the remaining part of the film experiences a confinement between two surfaces with a strong preference for the C component. The shift of phase boundaries in the symmetric case is approximately 2 grid points, which is smaller than the thickness of the wetting layer amounting to ∼4−5 grid points. From the coexistence of $C_{\perp}$ and $C_{||}$ in Figure 5b,c we see that the surface field value in those cases is just above or at the threshold necessary for the formation of the $C_{\perp}$ structure.

Influence of Interaction Parameters and the Effect of Confinement. In all thin films studied until now, we have used a fixed triple $\epsilon = (7.0, 8.0, 6.0)$ for the component−component interactions. We showed that in the bulk a core−shell gyroid structure appears to be quite robust in a wide range around this set of parameters. We now turn to the question how the thin film phase behavior is influenced by the strength of the interaction between the polymer components. The surface interactions are kept constant at $\epsilon_{M_0} = 7$ and $\epsilon_{M_1} = -5$, resulting in a strong preference of the C component both to the top surface and to the wetting layer at the substrate. Slight changes of the ϵ interaction parameters lead to major changes in the surface structures and their stability regions (Figure 7). As a reference, the phase diagram for the set of parameters of the previous sections $\epsilon = (7.0, 8.0, 6.0)$ is shown in Figure 7a, which is the same as in Figure 5c.

• $\epsilon = (6.0, 8.0, 7.0)$, Figure 7b: Exchanging the value of the interaction parameter between A and B with that between B and C leads to surface structures that are very similar in very thin films ($H < 9$). However, in thicker films, perforated lamellae form even at inter-

mediate film thicknesses. At commensurate film thicknesses, an AB mixed lamella coexists with PL.

• $\epsilon = (8.0, 8.0, 6.0)$, Figure 7c: Increasing the repulsion between the A and the B component leads to a phase diagram that is quite similar to the reference phase diagram (a). The phase boundaries are slightly shifted, and a coexistence of PL and $C_{||}$ is more favored in thicker films. Both the $C_{\perp}$ and the L phase are not found. At $H = 15$ and $H = 16$ the wetting layer at the substrate is laterally not continuous. Apparently the attraction of the B component to the substrate is not strong enough to compensate the repulsion between A and B.

• $\epsilon = (5.0, 9.0, 6.0)$, Figure 7d: Reducing the repulsion between the A and B component and increasing the repulsion between A and C leads to a phase diagram that is dominated by the PL phase. Apparently, the $C_{||}$ surface reconstruction is no longer favored. For very thin films, the behavior is similar to the reference system, except that $C_{\perp}$ is not found.

Although in the bulk the same microdomain structure is observed for different interaction parameters, the presence of confining walls leads to significant changes in the phase diagram and shifts of phase boundaries. As a function of the slit width and interaction parameters between the different components, a spectrum of surface structures is induced. For a rather large range of interaction parameters the system exhibits one symmetry in the bulk (gyroid structure), while under the influence of an external field (surface field) a number of structures with different symmetries are induced.

We already discussed this phenomenon of triblock terpolymers in the accompanying experimental paper.[32] In the experiments the situation is even more complex as the structure formation process takes place in concentrated solutions. Tiny differences in the vapor pressure of the solvent and the nature of the solvent have proven to significantly vary the microdomain structures in thin films, while in bulk the same structure was observed. Figure 9 in the experimental paper[32] shows for example four different types of cylindrical microdomain structures in thin films: core−shell cylinders, spheres-in-cylinders, cylinders-at-cylinders, and helices-at-cylinders.

Surface Reconstructions: AB Mixed Microdomain Structures. Finally, we concentrate on a system with $\epsilon = (6.4, 5.0, 4.5)$, where all component−component interaction parameters are smaller than in our reference system ($\epsilon = (7, 8, 6)$), confined between symmetric walls attracting the C block with $\epsilon_{M_0} = \epsilon_{M_1} = 4.75$. In the bulk, this system also forms a core−shell gyroid structure, where all three components are microphase-separated (Table 2). The choice for this system is inspired by the finding of AB mixed structures in bulk, upon decreasing the interaction parameter between A and C. Our results show that the surface field can also have an impact on the microphase separation of A and B. Figure 8a schematically shows the dependence of the surface structures on the film thickness: with increasing film thickness we find L, $C_{\perp}$, $L_{||}$, coexistence of $L_{||}$ and PL_1, PL_1, $C_{||}$, coexistence of $C_{||}$ and PL_2, PL_2, coexistence of $C_{||}$ and PL_2, $C_{||}$, and coexistence of $C_{||}$ and PL_3. The phase diagrams are quite similar to those shown in Figures 5a−c and 7; however, no wetting layer is formed at the substrate.

Besides the AB mixed lamellae at $H = 4$, the main difference to the phase diagrams in Figures 5 and 7 is

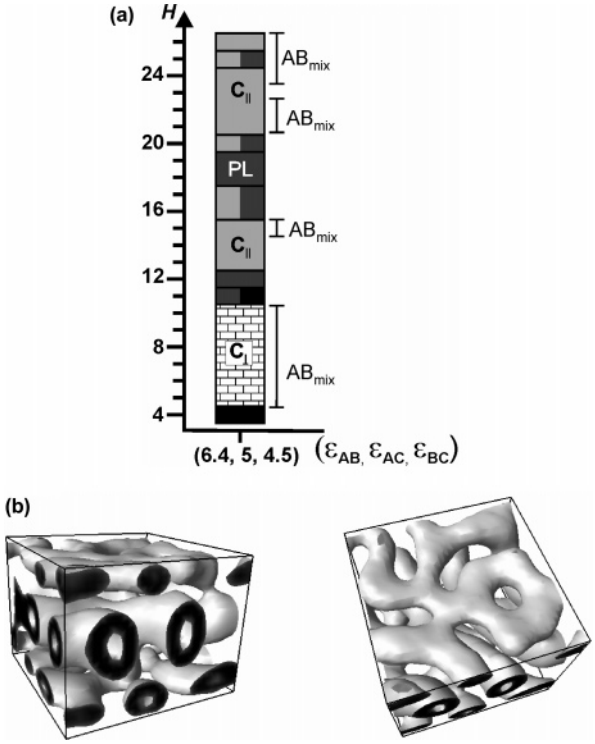

Figure 8. Surface reconstructions. The interaction parameters are $\epsilon = (6.4, 5.0, 4.5)$, $\epsilon_{M_0} = 4.75$, and $\epsilon_{M_1} = 4.75$. (a) Surface structures as a function of the film thickness. Color code: white, dis; light gray, $C_{||}$; dark gray, PL; black, L; tiled, $C_{\perp}$. (b) The isodensity surface of the B density is shown for $H = 25$.

that also other structures show mixing of A and B next to the surfaces. A typical example of this phenomenon is displayed in Figure 8b, where the isodensity surface of B is shown for $H = 25$. At both surfaces, the thickness of the surface structures is much smaller than that of the center structure, which shows a well-developed core−shell structure. A general rule seems to be that if the microdomain structures fit a certain film thickness, microphase separation occurs for all three components; if not, the microdomain structures next to the surfaces exhibit mixing of A and B. These structures are marked in the phase diagram. This interesting finding reveals the complex interplay between interaction parameters and confinement effects. We interpret this effect as a new type of surface reconstruction, in which the surface field not only induces a certain type of microdomain structure but also affects the degree of microphase separation of the block components. It leads to the mixed situation of apparent diblock microdomain structures close to the surface and core−shell triblock microdomain structures in the middle of the film.

Conclusion

We described the complex phase behavior of a specific ABC triblock terpolymer system confined between two walls. On the basis of the experimental results,[32] we were able to determine the interaction parameters between the components and the interaction parameters between the components and the interfaces. With this parametrization, a detailed match was found between the experimental results and our simulations based on SCF theory. Even details, like specific defect structures of the experiments, were found in the simulations. With increasing film thickness we observed a wetting layer

(W), cylinders oriented perpendicular to the film plane ($C_\perp$), parallel cylinders ($C_{||}$), perforated lamellae (PL), and again $C_{||}$. In analogy with earlier work on a two-component system,[23−25] we identified these structures as surface reconstructions of the core−shell gyroid structure in bulk. In particular, the core−shell PL structure can be seen as analogue to the PL surface reconstruction of cylinder-forming AB and ABA systems. New types of surface reconstruction observed in the studied ABC system are AB mixed L, PL, and $C_\perp$ surface structures.

We found that confined systems are very sensitive to small changes in the energetic interaction between the different components A, B, and C. While we observe a core−shell gyroid structure for a wide range of interaction parameters in bulk, confinement alters the phase behavior drastically. The stability region of the different phases is modulated by the film thickness via additivity of surface fields and commensurability effects. The presence of a wetting layer screens the surface field at that side, leading to microdomain structures which are mainly controlled by the surface field of the opposite wall.

Simulations like this might be used for identification of important experimental control parameters and eventually give design rules for ordering thin films. In particular, a combinatorial approach could provide a deeper insight in the complex interplay between surface field, interaction parameters, and confinement effects in thin films of triblock terpolymers.

Acknowledgment. We thank N. Rehse and A. Horvat for fruitful discussions and help. We acknowledge support from the Deutsche Forschungsgemeinschaft (SFB 481), the VolkswagenStiftung, and the NWO-DFG bilateral program.

References and Notes

(1) Mansky, P.; Chaikin, P.; Thomas, E. L. *J. Mater. Sci.* **1995**, *30*, 1987.
(2) Park, M.; Harrison, C.; Chaikin, P. M.; Register, R. A.; Adamson, D. H. *Science* **1997**, *276*, 1401.
(3) Park, C.; Yoon, J.; Thomas, E. L. *Polymer* **2003**, *44*, 6725.
(4) Anastasiadis, S. H.; Russell, T. P.; Satija, S. K.; Majkrzak, C. F. *Phys. Rev. Lett.* **1989**, *62*, 1852.
(5) Walton, D. G.; Kellogg, G. J.; Mayes, A. M.; Lambooy, P.; Russell, T. P. *Macromolecules* **1994**, *27*, 6225.
(6) Kellogg, G. J.; Walton, D. J.; Mayes, A. M.; Lambooy, P.; Russell, T. P.; Gallagher, P. D.; Satija, S. K. *Phys. Rev. Lett.* **1996**, *76*, 2503.
(7) Matsen, M. W. *Curr. Opin. Colloids* **1998**, *3*, 40.
(8) Binder, K. *Adv. Polym. Sci.* **1999**, *138*, 1.
(9) Fasolka, M. J.; Mayes, A. M. *Annu. Rev. Mater. Res.* **2001**, *31*, 323.
(10) Qi, S. Y.; Wang, Z. G. *Polymer* **1998**, *39*, 4639.
(11) Chen, H.; Chakrabati, J. *J. Chem. Phys.* **1998**, *39*, 4639.
(12) Feng, J.; Liu, H.; Hu, Y. *Macromol. Theory Simul.* **2002**, *11*, 556.
(13) Brown, G.; Chakrabarti, A. *J. Chem. Phys.* **1994**, *101*, 3310.
(14) Brown, G.; Chakrabarti, A. *J. Chem. Phys.* **1995**, *102*, 1140.
(15) Wang, Q.; Yan, Q. L.; Nealy, P. F.; de Pablo, J. J. *J. Chem. Phys.* **2000**, *112*, 450.
(16) Wang, Q.; Nealy, P. F.; de Pablo, J. J. *Macromolecules* **2001**, *34*, 3458.
(17) Szamel, G.; Müller, M. *J. Chem. Phys.* **2003**, *118*, 905.
(18) Sevink, G. J. A.; Zvelindovsky, A. V.; van Vlimmeren, B. A. C.; Maurits, N. M.; Fraaije, J. G. E. M. *J. Chem. Phys.* **1999**, *110*, 2250.
(19) Huinink, H. P.; Brokken-Zijp, J. C. M.; van Dijk, M. A.; Sevink, G. J. A. *J. Chem. Phys.* **2000**, *112*, 2452.
(20) Sevink, G. J. A.; Zvelindovsky, A. V.; Fraaije, J. G. E. M. In *Mesoscale Phenomena in Fluid Systems: ACS Symp. Ser.* **2003**, *861*, 258.
(21) Huinink, H. P.; van Dijk, M. A.; Brokken-Zijp, J. C. M.; Sevink, G. J. A. *Macromolecules* **2001**, *34*, 5325.
(22) Sevink, G. J. A.; Fraaije, J. G. E. M.; Huinink, H. P. *Macromolecules* **2002**, *35*, 1848.
(23) Knoll, A.; Horvat, A.; Lyakhova, K. S.; Krausch, G.; Sevink, G. J. A.; Zvelindovsky, A. V.; Magerle, R. *Phys. Rev. Lett.* **2002**, *89*, 035501.
(24) Knoll, A.; Magerle, R.; Krausch, G. *J. Chem. Phys.* **2004**, *120*, 1105.
(25) Horvat, A.; Lyakhova, K. S.; Sevink, G. J. A.; Zvelindovsky, A. V.; Magerle, R. *J. Chem. Phys.* **2004**, *120*, 1117.
(26) Lyakhova, K. S.; Sevink, G. J. A.; Zvelindovsky, A. V.; Horvat, A.; Magerle, R. *J. Chem. Phys.* **2004**, *120*, 1127.
(27) Pickett, G. T.; Balazs, A. C. *Macromol. Theory Simul.* **1998**, *7*, 249.
(28) Feng, J.; Ruckenstein, E. *Polymer* **2002**, *43*, 5775.
(29) Chen, H.-Y.; Fredrickson, G. H. *J. Chem. Phys.* **2002**, *116*, 1137.
(30) Ludwigs, S.; Böker, A.; Abetz, V.; Müller, A. H. E.; Krausch, G. *Polymer* **2003**, *44*, 6815.
(31) Ludwigs, S.; Böker, A.; Voronov, A.; Rehse, N.; Magerle, R.; Krausch, G. *Nat. Mater.* **2003**, *2*, 744.
(32) Ludwigs, S.; Schmidt, K.; Stafford, C.; Fasolka, M.; Karim, A.; Amis, E.; Magerle, R.; Krausch, G. *Macromolecules*, **2005**, *38*, 1850.
(33) Elbs, H.; Fukunaga, K.; Stadler, R.; Sauer, G.; Magerle, R.; Krausch, G. *Macromolecules* **1999**, *32*, 1204.
(34) Elbs, H.; Abetz, V.; Hadziioannou, G.; Drummer, C.; Krausch, G. *Macromolecules* **2001**, *34*, 7917.
(35) Elbs, H.; Drummer, C.; Abetz, V.; Krausch, G. *Macromolecules* **2002**, *35*, 5570.
(36) Fukunaga, K.; Elbs, H.; Magerle, R.; Krausch, G. *Macromolecules* **2000**, *33*, 947.
(37) Fukunaga, K.; Hashimoto, T.; Elbs, H.; Krausch, G. *Macromolecules* **2002**, *35*, 4406.
(38) Fukunaga, K.; Hashimoto, T.; Elbs, H.; Krausch, G. *Macromolecules* **2003**, *36*, 2852.
(39) Fraaije, J. G. E. M. *J. Chem. Phys.* **1993**, *99*, 9202.
(40) van Vlimmeren, B. A. C.; Maurits, N. M.; Zvelindovsky, A. V.; Sevink, G. J. A.; Fraaije, J. G. E. M. *Macromolecules* **1999**, *32*, 646.
(41) Maurits, N. M.; Fraaije, J. G. E. M.; Altevogt, P.; Evers, O. A. *Comput. Theor. Polym. Sci.* **1996**, *6*, 1.
(42) Fraaije, J. G. E. M.; van Vlimmeren, B. A. C.; Maurits, N. M.; Postma, M.; Evers, O. A.; Hoffmann, C.; Altevogt, P.; GoldbeckWood, G. *J. Chem. Phys.* **1997**, *106*, 4260.
(43) Zvelindovsky, A. V.; Sevink, G. J. A.; Fraaije, J. G. E. M. *Phys. Rev. E* **2000**, *62*, R3063.
(44) Henkee, C. S.; Thomas, E. L.; Fetters, L. J. *J. Mater. Sci.* **1988**, *23*, 1685.
(45) Rehse, N.; Knoll. A.; Konrad, M.; Magerle, R.; Krausch, G. *Phys. Rev. Lett.* **2001**, *87*, 035505.

MA049047L